



ROCK-dependent phosphorylation of NUP62 regulates p63 nuclear transport and squamous cell carcinoma proliferation

Masaharu Hazawa^{1,2,3,†,*} , De-Chen Lin^{4,5,†}, Akiko Kobayashi², Yan-Yi Jiang⁴, Liang Xu⁴, Firli Rahmah Primula Dewi², Mahmoud Shaaban Mohamed², Hartono², Mitsutoshi Nakada^{1,6}, Makiko Meguro-Horike⁷, Shin-ichi Horike^{1,7}, H Phillip Koeffler^{4,5} & Richard W Wong^{1,2,3,**} 

Abstract

p63, more specifically its Δ Np63 α isoform, plays essential roles in squamous cell carcinomas (SCCs), yet the mechanisms controlling its nuclear transport remain unknown. Nucleoporins (NUPs) are a family of proteins building nuclear pore complexes (NPC) and mediating nuclear transport across the nuclear envelope. Recent evidence suggests a cell type-specific function for certain NUPs; however, the significance of NUPs in SCC biology remains unknown. In this study, we show that nucleoporin 62 (NUP62) is highly expressed in stratified squamous epithelia and is further elevated in SCCs. Depletion of NUP62 inhibits proliferation and augments differentiation of SCC cells. The impaired ability to maintain the undifferentiated status is associated with defects in Δ Np63 α nuclear transport. We further find that differentiation-inducible Rho kinase reduces the interaction between NUP62 and Δ Np63 α by phosphorylation of phenylalanine–glycine regions of NUP62, attenuating Δ Np63 α nuclear import. Our results characterize NUP62 as a gatekeeper for Δ Np63 α and uncover its role in the control of cell fate through regulation of Δ Np63 α nuclear transport in SCC.

Subject Categories Cancer; Membrane & Intracellular Transport

DOI 10.15252/embr.201744523 | Received 23 May 2017 | Revised 26 October 2017 | Accepted 6 November 2017 | Published online 7 December 2017

EMBO Reports (2018) 19: 73–88

See also: **J Borlido & MA D'Angelo** (January 2018)

Introduction

Squamous cell carcinomas (SCCs) are lethal malignancies arising from the stratified epithelia of skin, esophagus, cervix, and the head and neck. Genomic analysis of SCCs identified genomic amplification of *TP63* in up to 30% of tumors, with overexpression of its mRNA in the majority of SCCs [1–4].

TP63, a p53 homolog, is a master transcriptional regulator of epithelial development and maintenance [5–12]. Deletion of *TP63* during embryogenesis resulted in the absence of skin and limbs [5,6]. *TP63* contains two different promoters to drive two distinct isoform classes either with or without N-terminal transactivation domain, TAp63 and Δ Np63, respectively [9–11]. In addition, both TAp63 and Δ Np63 have three variants with different C-termini (α , β , and γ) generated by alternative splicing [9–11]. Δ Np63 α is the prominent isoform in adult epidermis [7,13,14], where it contributes to self-renewal ability or stemness [5–8,15–17]. Of note, pharmacological inhibition of ROCK, a differentiation-inducible serine/threonine kinase [18,19], resulted in induction of continuous proliferation ability with elevated Δ Np63 α expression in keratinocytes [20].

In the context of cancer, the major isoform of p63 detected in SCC is also Δ Np63 α [21–25]. Δ Np63 α functions as a transcriptional regulator of different gene subsets [13,26,27]. Forced expression of Δ Np63 α was sufficient to drive proliferation and tumorigenesis [24], while inducible genetic deletion of *TP63* blocked chemical-induced SCC formation [23], underscoring Δ Np63 α as an oncogenic transcription factor in SCCs. Although the role of Δ Np63 α has been established, the process controlling Δ Np63 α nuclear transport remains poorly understood.

The nuclear pore complex (NPC) is the sole gateway between the nucleus and the cytoplasm [28–33]. NPCs consist of multiple copies of roughly 30 different proteins known as nucleoporins (NUPs).

1 Cell-Bionomics Research Unit, Innovative Integrated Bio-Research Core, Institute for Frontier Science Initiative, Kanazawa University, Kanazawa, Ishikawa, Japan

2 Laboratory of Molecular Cell Biology, School of Natural System, Institute of Science and Engineering, Kanazawa University, Kanazawa, Ishikawa, Japan

3 WPI Nano Life Science Institute (WPI-NanoLSI), Kanazawa University, Kakuma-machi, Kanazawa, Japan

4 Cancer Science Institute of Singapore, National University of Singapore, Singapore, Singapore

5 Division of Hematology/Oncology, Cedars-Sinai Medical Center, Los Angeles, CA, USA

6 Department of Neurosurgery, Graduate School of Medical Science, Kanazawa University, Kanazawa, Ishikawa, Japan

7 Advanced Science Research Center, Institute for Gene Research, Kanazawa University, Kanazawa, Ishikawa, Japan

*Corresponding author. Tel: +81 0762646253; E-mail: masaharu.akj@gmail.com

**Corresponding author. Tel: +81 0762646253; E-mail: rwong@staff.kanazawa-u.ac.jp

† These authors contributed equally to this work

About one-third of NUPs, including NUP62, contain unstructured phenylalanine–glycine (FG) repeats, which form a soft and flexible cobweb composed of ~200 intrinsically disordered polypeptide chains, mediating selective nucleocytoplasmic transport [34,35]. Recently, new evidence suggests that NPC composition varies among different cell types and tissues, and this heterogeneity is required for distinct biological processes such as muscle development, neurogenesis, and embryonic stem cell pluripotency [36–41]. Importantly, single NUP mutation resulted in developmental defects and diseases [42], highlighting the significant role of NUPs in maintaining tissue homeostasis. However, whether and how NUPs are involved in the biology of stratified squamous epithelia remains largely unknown.

Here, we demonstrate that the expression of NUP62, one of FG-NUPs, is abundant in stratified epithelia. Aberrant overexpression of NUP62 is evident in human SCCs. NUP62 expression is required to maintain undifferentiated status of SCCs through regulating Δ Np63 α nuclear transport. Mechanistically, pro-differentiation ROCK kinase negatively regulates this Δ Np63 α nuclear transport by limiting the interaction between Δ Np63 α and NUP62 through phosphorylation of the FG regions of NUP62.

Results

Identification of NUP62 as a novel differentiation-preventing factor in SCC

To explore the expression profile of NUPs in healthy human tissues, we re-analyzed RNA-seq data from The Human Protein Atlas (see Materials and Methods). The transcript levels of six NUPs (NUP107, NUP85, NUP62, NUP54, NUP188, and TPR) were higher in representative stratified epithelia, skin, and esophagus relative to other NUPs (Fig 1A). Among them, NUP62 was the only gene displaying increased expression during induction of the epidermal lineage (Fig 1B). To examine expression profile of NUP62 in skin tissue, we performed immunofluorescent confocal microscopic analysis using healthy human skin sample (Fig 1C). We found that NUP62 was expressed in the undifferentiated layer, indicating NUP62 is expressed in the progenitor population.

In order to determine the expression profile of NUPs in SCC, we compared the expression of above six NUPs mRNAs in normal

versus tumor samples using data from both the RNA-sequencing from The Cancer Genome Atlas (TCGA) and the cDNA microarray data from Gene Expression Omnibus (GEO; series GSE7410). We found that NUP62 was the top gene with consistent overexpression in primary SCC samples from both head and neck (Fig 1D) and cervix (Fig 1E).

To dissect the role of the above six NUPs in SCC growth, we individually silenced expression of each NUP (Figs 1F and EV1A), and identified that NUP62 is required for the proliferation of SCC cells (Figs 1G and EV1B). Next, we investigated whether other highly expressed NUPs in SCCs (NUP62, NUP107, NUP85, and NUP54) regulate epidermal differentiation. We queried TCGA datasets to determine co-expression profiles among these NUPs and epidermal differentiation genes such as IVL and small proline-rich protein 1B (SPRR1B). NUP62 was the only NUP showing an inverse correlation with both IVL and SPRR1B (Pearson Score < -0.3; Fig 1H). Moreover, NUP62 depletion activated these epidermal differentiation genes, a result not observed in any other NUPs (Fig 1I). Taken together, these data strongly suggest that NUP62 has cell type-specific function to prevent epidermal differentiation induction in SCCs.

NUP62 is required for the proliferation and prevent of differentiation of SCC cells

To study the biological role of NUP62 in SCC, we silenced NUP62 in a number of cell lines from cervical SCC (CSCC) and head and neck SCC (HNSCC) by siRNA-mediated knockdown (Fig 2A). Notably, silencing of NUP62 strongly inhibited the proliferation of various types of SCC cells (Fig 2B). Several cell lines, including ME-180, UMSSC1, and Ca9-22, barely grew in the absence of NUP62. Similarly, shRNA-mediated NUP62 depletion resulted in significant reduction in short-term cell proliferation and foci formation of SCC cells (Fig EV1C–E).

As lack of differentiation is a hallmark of SCC, we measured levels of molecular markers associated with squamous cell differentiation such as SPRR1B, IVL, filaggrin (FLG), and loricrin (LOR). Silencing NUP62 enhanced the expression of these genes (Fig 2C). Interrogation of TCGA RNA-seq datasets showed that expression levels of these differentiation related genes are inversely related to levels of NUP62 (Fig 2D). Taken together, these data strongly suggest that NUP62 is a functional requisite for SCCs.

Figure 1. Identification of NUP62 as epidermal differentiation-preventing factor in SCC.

- Heat map representing NUPs transcript levels across healthy tissues including skin, esophagus, bone marrow, brain, muscle, salivary gland, pancreas and liver from The Human Protein Atlas (see URLs).
- Human H1 embryonic stem cells were differentiated to keratinocyte progenitors *in vitro*, and their global RNA expression profiles during differentiation were analyzed using RNA-seq. Rectangle highlights NUP62.
- Expression profiles of NUP62 and IVL in normal skin tissue. Bar = 30 μ m.
- Heat map showing the expression of NUP62 in non-tumor tissue, and primary head and neck squamous cell carcinoma (HNSCC) samples from TCGA. SI, SII, SIII, SIV denote stages I, II, III and IV.
- NUPs expression levels in cervical squamous cell carcinoma (CSCC) samples. NUP62 mRNA levels were retrieved from GEO (accession number is shown above the figure). Five data in healthy human samples (M) and 40 data in tumor patients (T). *P* values are based on unpaired two-tailed *t*-test with **indicating *P* < 0.01. n.s. indicates not significant.
- Western blot analysis of each NUP in SCC cells at 72 h after siRNA-mediated knockdown.
- Plot showing the correlation between average effect of NUP depletion on SAS cell growth and differential gene expression (normal tissue versus HNSCC from TCGA). NUP62 was highlighted in orange. TP63 was marked in purple as positive control for oncogene. Data show mean from two independent experiments (*n* = 2).
- Summary of correlation coefficient between each NUPs mRNA and epidermal differentiation genes (SPRR1B and IVL) in head and neck SCC from TCGA.
- qRT-PCR analysis of genes associated with epidermal differentiation after individual depletion of each NUPs. Transcripts of each gene with scrambled siRNAs is considered 1.0. Data show mean \pm SD (*n* = 3; NUP62) or mean (*n* = 2; others). *P* values are based on one sample *t*-test with *indicating *P* < 0.05.

Source data are available online for this figure.

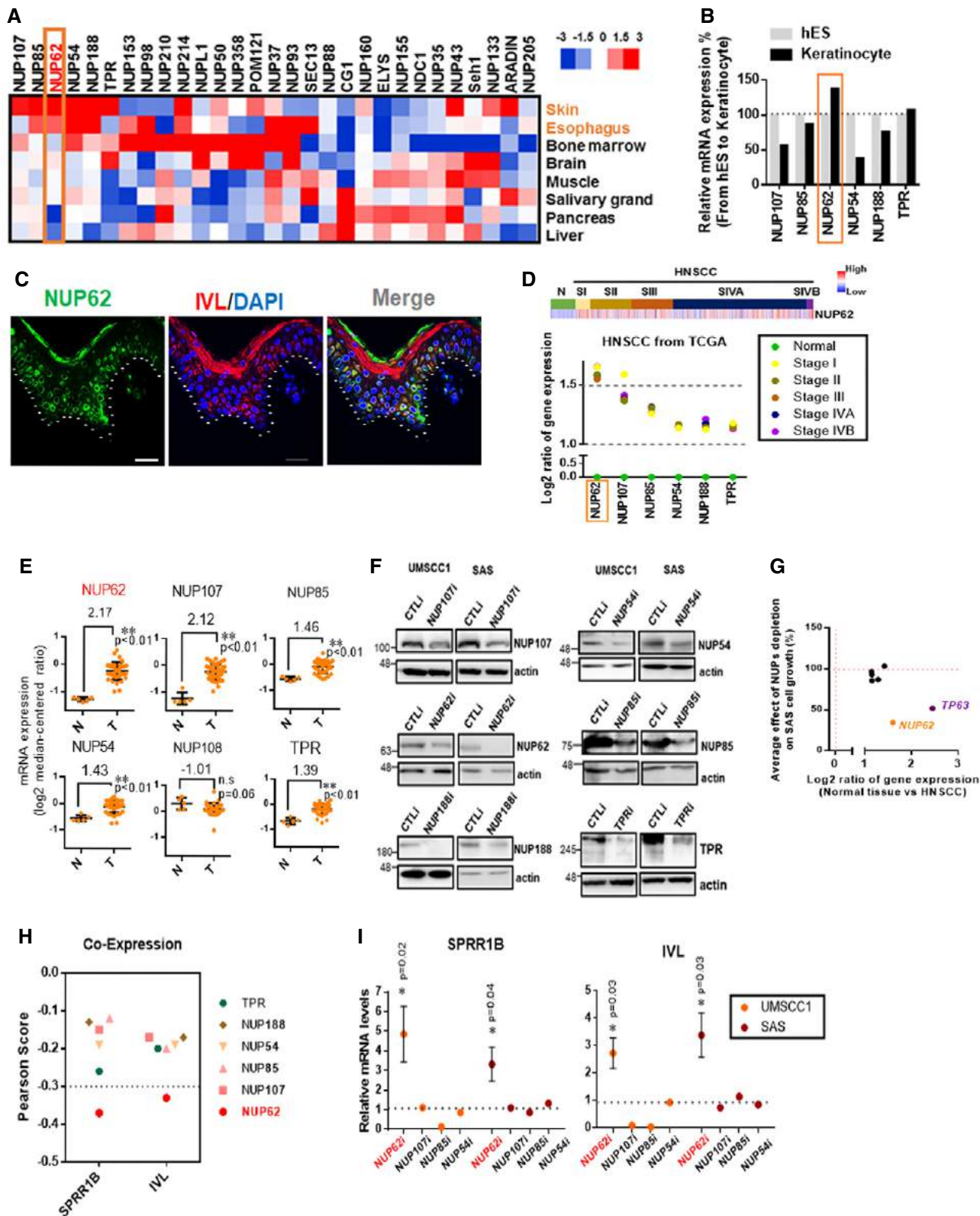


Figure 1.

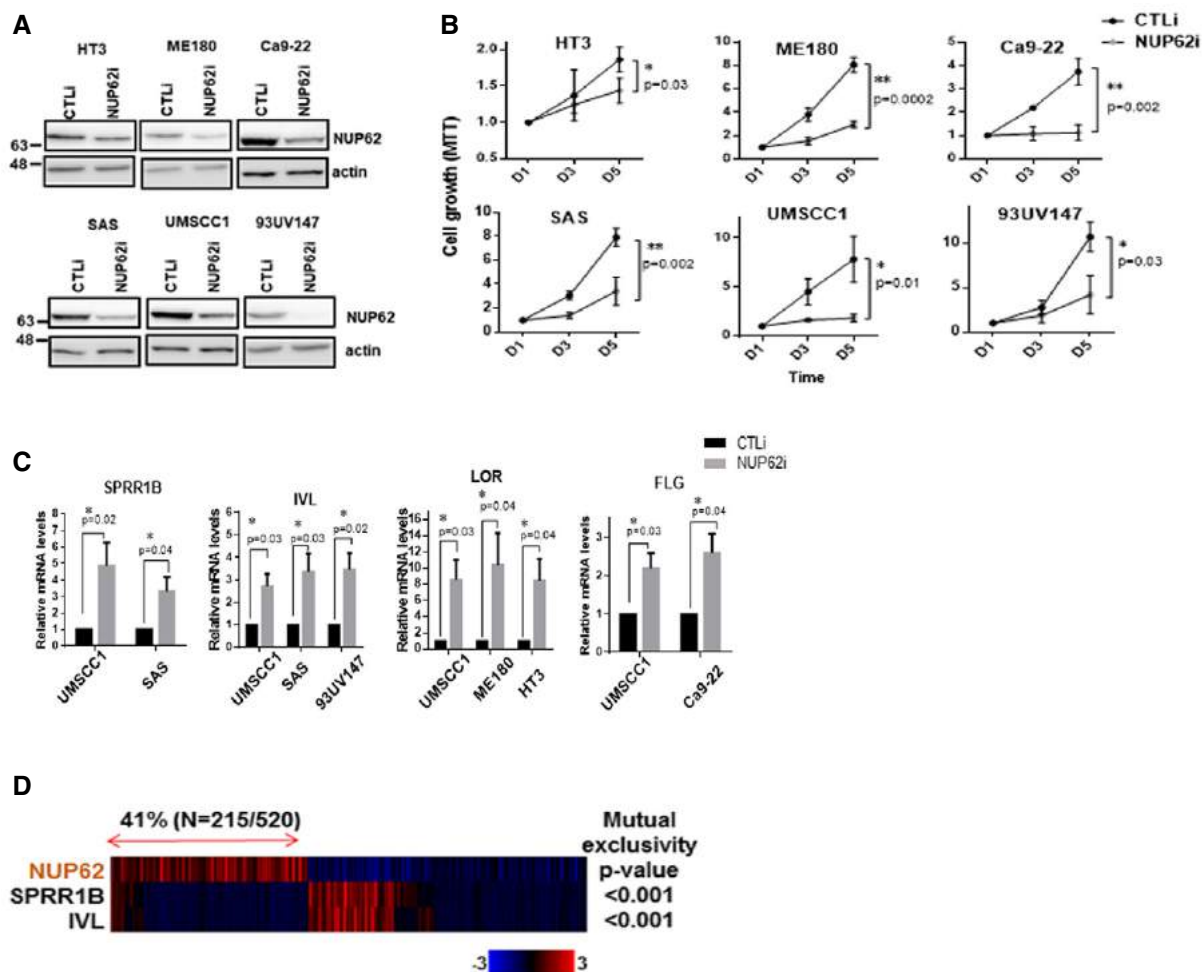


Figure 2. NUP62 is required for proliferation and undifferentiated status of SCC cells.

A Western blot analysis of NUP62 in SCC cells after siRNA-mediated NUP62 depletion.

B Proliferation of NUP62-silenced SCC cells examined by MTT assay. Data show mean \pm SD from three independent experiments ($n = 3$). P values are based on unpaired two-tailed t -test with *indicating $P < 0.05$ and ** $P < 0.01$.

C qRT-PCR analysis of differentiation related genes in SCC cell line treated with scrambled siRNAs (CTLi) or NUP62 siRNAs (NUP62i). Data show mean \pm SD from three independent experiments ($n = 3$). P values are based on one sample t -test with *indicating $P < 0.05$.

D Heat map showing mutual exclusivity between NUP62 expression and differentiation related genes. Samples were divided according to mRNA expression levels [mRNA expression z-scores (RNA-Seq V2 RSEM) $>$ mean + 0.1 SD] from the TCGA cohorts. P values are based on fisher exact test.

Source data are available online for this figure.

Transcriptome analysis of NUP62-regulated genes and processes

To delineate the SCC-associated functions of NUP62, cDNA microarray was performed in UMSSC1 cells comparing the silencing of the protein versus control cells. Loss of NUP62 altered the expression of 2,019 genes compared to control (twofold change, Fig 3A). Activated genes after NUP62 silencing were enriched in Gene Ontology terms related to phosphorylation, regulation of localization, Rho guanine nucleotide exchange factors (GEF), negative regulation of cell proliferation, epithelial cell differentiation, and regulation of transport (Fig 3B). Interestingly, gene set enrichment analysis (GSEA) identified a strong correlation between down-regulated genes in NUP62-silenced cells and those in p63-depleted SCCs (GSE88833; Fig 3C). As NUP62 depletion did not affect the level of

Δ Np63 α transcript *per se* (Fig 3D and E). We next explored alternative mechanisms underlying this molecular association.

NUP62 regulates Δ Np63 α nuclear transport in SCCs

To examine whether NUP62 affects p63 localization, we quantified the amount of nuclear and cytoplasmic Δ Np63 α using confocal microscopy. Attenuated nuclear Δ Np63 α level was detected in NUP62-depleted SCC cells (Fig 4A and B). Concordantly, nuclear-cytoplasmic fractionation demonstrated that Δ Np63 α abundance in the nuclear fraction was less in the NUP62 silenced SCC cells compared to the control cells (Fig 4C).

To investigate whether the amount of nuclear Δ Np63 α affects its transcription activity, we performed qRT-PCR analysis to detect

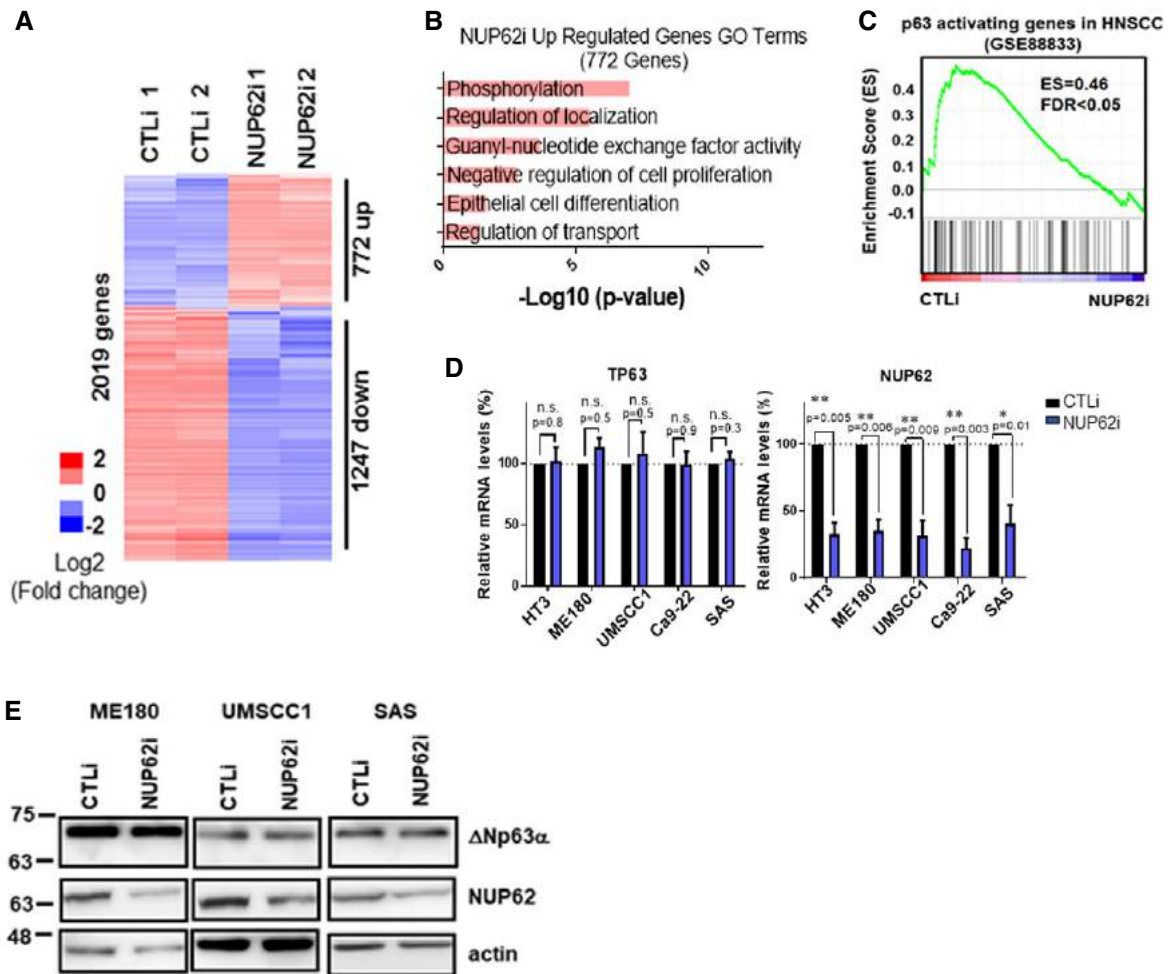


Figure 3. Transcriptome analysis of NUP62-regulated genes and processes.

- A Heat map from microarray data showing up- and down-regulated genes after 3 days of knockdown of NUP62.
 B GO analysis of the up-regulated genes upon NUP62 depletion.
 C GSEA of NUP62 knockdown microarray datasets with down-regulated genes in HNSCC cell upon p63 knockdown (GSE88833).
 D qRT-PCR analysis of p63 and NUP62 mRNA in various SCC cell lines depleted of NUP62. Expression levels of cells treated with scrambled siRNAs is considered 100%. Data show mean \pm SD from three independent experiments ($n = 3$). P values are based on one sample t-test with *indicating $P < 0.05$ and ** $P < 0.01$.
 E Western blot analysis of Δ Np63 α in SCC cells after siRNA-mediated NUP62 depletion.

Source data are available online for this figure.

mRNA levels of Δ Np63 α target genes (Fig 4D). The transcription levels of well-defined Δ Np63 α targets (EGFR [43], ADA [44], PERP [45], EDAR [46], ZNF750 [47,48], WWC1 [25], PUMA [22], CDKN1A [49], IHH [50], GLI2 [51], and SMAD7 [52]) significantly changed upon NUP62 knockdown (Fig 4E). Of note, TP63 target genes (such as FN1 [26], FAS, and SKT11 [53]) showed undetectable changes (Fig EV2). Collectively, these results suggest that NUP62 mediates Δ Np63 α nuclear transport.

ROCK pathway negatively regulates Δ Np63 α nuclear transport in human SCCs

As previous study suggested that MAP kinase-dependent phosphorylation of certain NUPs leads to their nuclear transport [54], we explored whether protein phosphorylation pathway was involved

in NUP62-dependent Δ Np63 α nuclear transport. Notably, our pathway enrichment analysis found that focal adhesion was the top signaling pathway affected by silencing of NUP62 (Fig 5A), and GSEA confirmed that NUP62-regulated genes were associated with a “genes controlled by ROCK” (GSE61226) signature (Fig 5B). Since ROCK pathway is downstream of the focal adhesion pathway and is regulated by rho GEF [55], we sought to determine whether ROCK activity influenced Δ Np63 α nucleocytoplasmic transport. Confocal microscopy analysis showed that inhibition of ROCK pathway by Y27632 significantly increased nuclear Δ Np63 α amounts (Fig 5C). Consistent with elevated Δ Np63 α level in nucleus, Y27632 treatment modulated transcript amount of target genes of Δ Np63 α (Fig 5D). On the other hand, ROCK activation by overexpressing a constitutive active ROCK1, Δ 3-ROCK1 [56], inhibited Δ Np63 α nuclear accumulation (Fig 5E and F), which

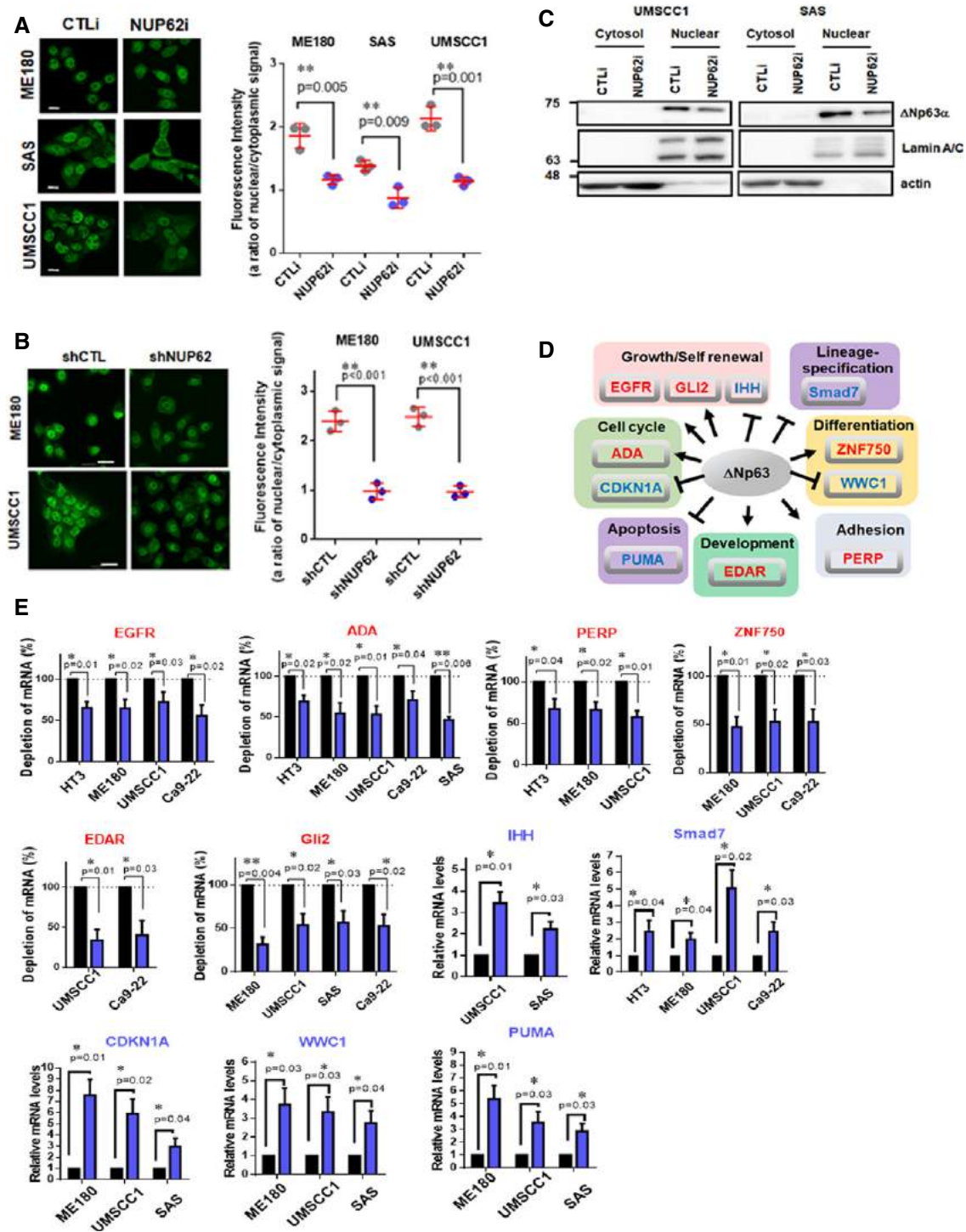


Figure 4. NUP62 regulates Δ Np63 α nuclear transport in SCCs.

A, B Immunofluorescence confocal microscopic analysis of Δ Np63 α in SCC cells after transient depletion of NUP62 by siRNA (72 h post transfection), (A) and shRNA (B). Representative pictures [bar: 10 μ m (A) and 20 μ m (B)] and the quantifications as ratio of nuclear/cytoplasm signals were presented as scatter plot with mean \pm SD from three independent experiments ($n = 3$). P values are based on unpaired two-tailed t -test with *indicating $P < 0.05$ and ** $P < 0.01$.

C Western blot analysis of Δ Np63 α protein levels in cytosol and nuclear fractions of SCC cells depleted NUP62.

D Transcriptional targets of Δ Np63 α , grouped according to their known functions. Red; activated genes, Blue; suppressed genes.

E qRT-PCR analysis of Δ Np63 α target genes mRNA in SCC cells depleted NUP62. Expression levels of cells treated with scrambled siRNAs is considered 100%. Data show mean \pm SD from three independent experiments ($n = 3$). P values are based on one sample t -test with *indicating $P < 0.05$ and ** $P < 0.01$.

Source data are available online for this figure.

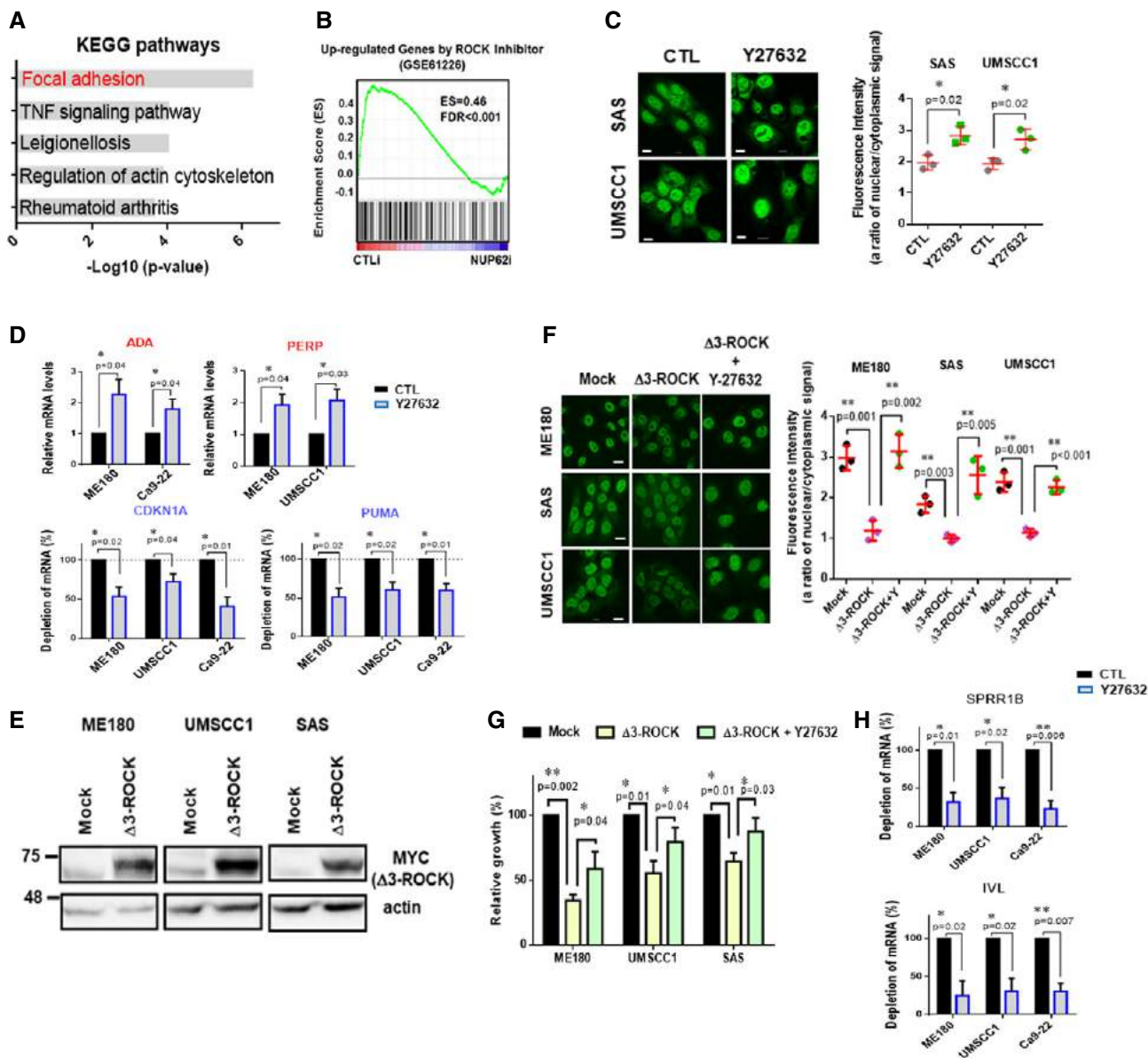


Figure 5. ROCK kinase inhibits Δ Np63 α nuclear transport in SCCs.

- A Pathway analysis of the up-regulated genes upon NUP62 depletion.
- B GSEA after NUP62 knockdown with up-regulated genes by ROCK inhibition microarray datasets (GSE61226).
- C Immunofluorescence confocal microscopic analysis of Δ Np63 α in SCC cells treated with ROCK1 inhibitor (Y27632, 10 μ M, 24 h). Representative pictures (bar: 10 μ m) and quantification as a ratio of nuclear/cytoplasm signals presented as a scatter plot with mean \pm SD from three independent experiments ($n = 3$). P value are based on unpaired two-tailed t -test with *indicating $P < 0.05$.
- D qRT-PCR analysis of Δ Np63 α target genes mRNA in SCC cells after Y27632 treatment (24 h, 10 μ M). Expression levels of cells treated with scrambled siRNAs is considered 100%. Data show mean \pm SD from three independent experiments ($n = 3$). P values are based on one sample t -test with *indicating $P < 0.05$.
- E Western blot analysis of exogenous constitutively active form of ROCK1 (Δ 3-ROCK).
- F Immunofluorescence confocal microscopic analysis of Δ Np63 α in SCC cells expressing Δ 3-ROCK1 and the effect of ROCK inhibitor (Y27632, 10 μ M, 24 h). Representative pictures (bar: 10 μ m) and quantification as a ratio of nuclear/cytoplasm signals presented as a scatter plot with mean \pm SD from three independent experiments ($n = 3$). P values are based on unpaired two-tailed t -test with **indicating $P < 0.01$.
- G Proliferation of SCC cells expressing Δ 3-ROCK1 and effect of Y27632 (10 μ M, analyzed by MTT assay). Data show mean \pm SD from three independent experiments ($n = 3$). P values are based on unpaired two-tailed t -test with *indicating $P < 0.05$, and ** $P < 0.01$.
- H qRT-PCR analysis of IVL and SPRR1B mRNA in SCC cells treated with Y27632. Expression levels of cells with DMSO is considered 100%. Data show mean \pm SD from three independent experiments ($n = 3$). P values are based on one sample t -test with *indicating $P < 0.05$ and ** $P < 0.01$.

Source data are available online for this figure.

was rescued by a ROCK inhibitor (Y-27632) but not by inhibitor of CRM1, another major nuclear transporter (Fig EV3A), suggesting that ROCK pathway regulates Δ Np63 α -importing process rather than Δ Np63 α -exporting processes.

Because Δ Np63 α promotes the malignant phenotypes of SCCs [16,26,27], we asked whether the ROCK pathway affected SCC growth potential. Blockade of ROCK activity using Y-27632 significantly enhanced SCC growth (Fig EV3B and C), whereas Δ 3-ROCK1 expression resulted in the opposite effect (Figs 5G and EV3D). We further observed that Y27632 treatment rescued the impaired proliferation induced by Δ 3-ROCK1 (Figs 5G and EV3D). Importantly, Y27632 treatment inhibited molecular markers associated with squamous cell differentiation such as IVL and SPRR1B (Fig 5H), supporting the role of the ROCK pathway as a differentiation-inducible serine/threonine kinase [18–20]. Taken together, these results suggest that ROCK pathway compromised differentiation status of SCCs potentially by limiting Δ Np63 α nuclear transport.

Phosphorylation of FG domain of NUP62 mediates the interaction between Δ Np63 α and NUP62

In order to elucidate Δ Np63 α nuclear transport system, we first addressed whether it involves nuclear transport receptors (NTRs). Since nuclear localization signal (NLS), an amino acid sequence consisting of positively charged lysines (K) or arginines (R), tags proteins for NTR-mediated traffic [57], we searched for nuclear localization signal (NLS) on Δ Np63 α . Based on NLS mapper (http://nls-mapper.iab.keio.ac.jp/cgi-bin/NLS_Mapper_form.cgi), two potential NLSs was found in Δ Np63 α (Fig 6A). To explore the biological functions of those candidate NLSs, we generated full-length Δ Np63 α (Δ Np63 α^{WT}), NLS1-deleted Δ Np63 α (Δ Np63 α^{ANLS1}), and NLS2-deleted Δ Np63 α (Δ Np63 α^{ANLS2}), all of which were fused with GFP at the C-terminus (Fig 6A). Quantification by fluorescent confocal microscopy showed that the vast majority of Δ Np63 α^{WT} and Δ Np63 α^{ANLS2} localized in the nucleus (Fig 6B). In contrast, ~30% cells expressing Δ Np63 α^{ANLS1} exhibited signals in both the cytosol and nucleus (Fig 6C). Importantly, NLS1 sequence on Δ Np63 showed high similarity with validated NLS of both p53 and

p73 (Fig 6D) [58–60], suggesting that Δ Np63 nuclear import is mediated through NLS1.

As importin β /karyopherin β (KPNB1) plays a key role in NLS-mediated nuclear traffic, we asked whether KPNB1 depletion affects Δ Np63 α nuclear transport. We confirmed that KPNB1 is expressed in all cell lines tested, while Δ Np63 α is specific for SCC cells (Fig EV4A). Importantly, depletion of KPNB1 significantly decreased Δ Np63 α nuclear import in SCC cells, indicating that KPNB1 mediates Δ Np63 α nuclear traffic (Fig 6E and F). Collectively, these results suggest that Δ Np63 nuclear transport is mediated by KPNB1-dependent pathway.

NUP62 harbors FG repeated region in N-terminus required for nucleocytoplasmic regulating factors, and coiled-coil (CC) domain in C-terminus to bind with NUP54 [61] (Fig 6G). To explore the basis for the functional relationship between ROCK1 pathway and NUP62-dependent Δ Np63 α nuclear transport, we constructed NUP62 fragments and performed immunoprecipitation (IP) analysis to determine p63-interacting regions on NUP62 (Fig 6G). Of note, Δ Np63 α preferably bound to the FG region (Fig 6H). Analysis of PhosphoSitePlus (see Materials and Methods) revealed that the FG domain of NUP62 includes potential phosphorylation sites, S2 and T20 (Fig 6H), which are highly conserved (Fig EV4B). Next, in order to examine whether the ROCK1 pathway phosphorylates FG domain, Δ 3-ROCK1 was co-expressed with the FG fragment, and cell lysates were immuno-precipitated with anti-GFP antibodies and then immunoblotted with phosphor-serine/threonine antibody (Fig 6I). Co-expression of the FG domain fragment and Δ 3-ROCK1 resulted in a prominent enrichment of FG domain fragments having elevated phosphorylation (Figs 6I and EV4C). Importantly, this phosphorylated FG domain fragment had decreased interaction with Δ Np63 α (Fig 6J). To explore further the biological relevance of the phosphorylation on FG domain of NUP62, we generated an alanine replaced mutant (Amt) NUP62 (Fig EV4D). Importantly, point mutations of the phosphorylation sites (S2A and T20A) enhanced the interaction between NUP62 and Δ Np63 α (Fig 6K), suggesting the phosphorylation of FG domain of NUP62 decreased the interaction between NUP62 and Δ Np63 α .

Figure 6. ROCK1-dependent phosphorylation on the FG domain of NUP62 decreases the Δ Np63 α –NUP62 interaction.

- A Schematic representation of the structural and functional domains of Δ Np63 α . DBD, DNA binding domain; OD, Oligomerization; TA, Transactivation; SAM, Steric a-motif; TID, transactivation inhibitory domain (upper panel). Predicted NLSs in Δ Np63 α by NLS mapper (middle panel). Diagram of mutations conducted in Δ Np63 α (bottom panel).
- B, C Immunofluorescence confocal microscopic analysis of Δ Np63 α^{WT} , Δ Np63 α^{ANLS1} and Δ Np63 α^{ANLS2} in 293T. Representative pictures are shown (B). Bar indicates 10 μ m. Phenotypes are quantified by counting [$n = 2$, (C)].
- D Comparison of NLS score p53, p73 and p63.
- E Western blot analysis of KPNB1 in SCC cells after siRNA knockdown.
- F Immunofluorescence confocal microscopic analysis of Δ Np63 α in KPNB1 silenced SCC cells. Representative pictures (bar: 10 μ m) and quantification as a ratio of nuclear/cytoplasm signals presented as scatter plot with mean \pm SD from three independent experiments ($n = 3$). P values are based on unpaired two-tailed t -test with *indicating $P < 0.05$.
- G Schematic representation of the structural and functional domains of NUP62. FG., FG repeat, CC., coiled-coil domain.
- H Schematic representation of NUP62 GFP fusion constructs overexpressed in HEK293T cells. HEK293T cells were co-transfected with Flag-tagged Δ Np63 α and GFP-fused NUP62 fragments (FG, Middle, and CC as shown in right panel). Seventy-two hours after transfection, cells were harvested, lysed, followed by immunoprecipitation (IP) assay using an anti-Flag antibody. Potential phosphorylation sites on FG is indicated.
- I, J HEK293T cells were co-transfected with FG, Δ 3-ROCK1 (I), together with Flag-tagged Δ Np63 α (J). Twenty-four hours after transfection, cells were treated with Y27632 (24 h, 10 μ M). At 72 h after transfection, cells were harvested, lysed, and proceeded for IP assay using indicated antibody.
- K Interaction between ectopic NUP62 and Δ Np63 α is shown either with wild-type NUP62 (WT) or with a point mutation in the S2 and T20 of FG (Amt).

Source data are available online for this figure.

ΔNp63α nuclear transport is mediated by the phosphorylation of FG domain of NUP62

Finally, we performed confocal microscopy analysis to measure p63 nucleocytoplasmic transport in a variety of SCC cells expressing either WT or Amt NUP62 (Fig 7A) including overexpressed Δ3-ROCK1 (Fig 7B and C). Mutant NUP62 showed increased ΔNp63α levels in the nucleus compared to WT NUP62 (Fig 7C). Of

note, Δ3-ROCK1 overexpression failed to compromise ΔNp63α nuclear importing ability of Amt NUP62, suggesting the phosphorylation of FG (S2/T20 sites) of NUP62 is crucial for ΔNp63α nuclear importation (Fig 7C). In parallel, this elevated ΔNp63α in the nucleus modulated the level of transcript of ΔNp63α target genes (Fig EV5A). Both WT and Amt NUP62 proteins co-localized with another NPC molecule RanBP2 [62], suggesting those ectopic NUP properly localized on the nuclear envelope (Fig EV5B).

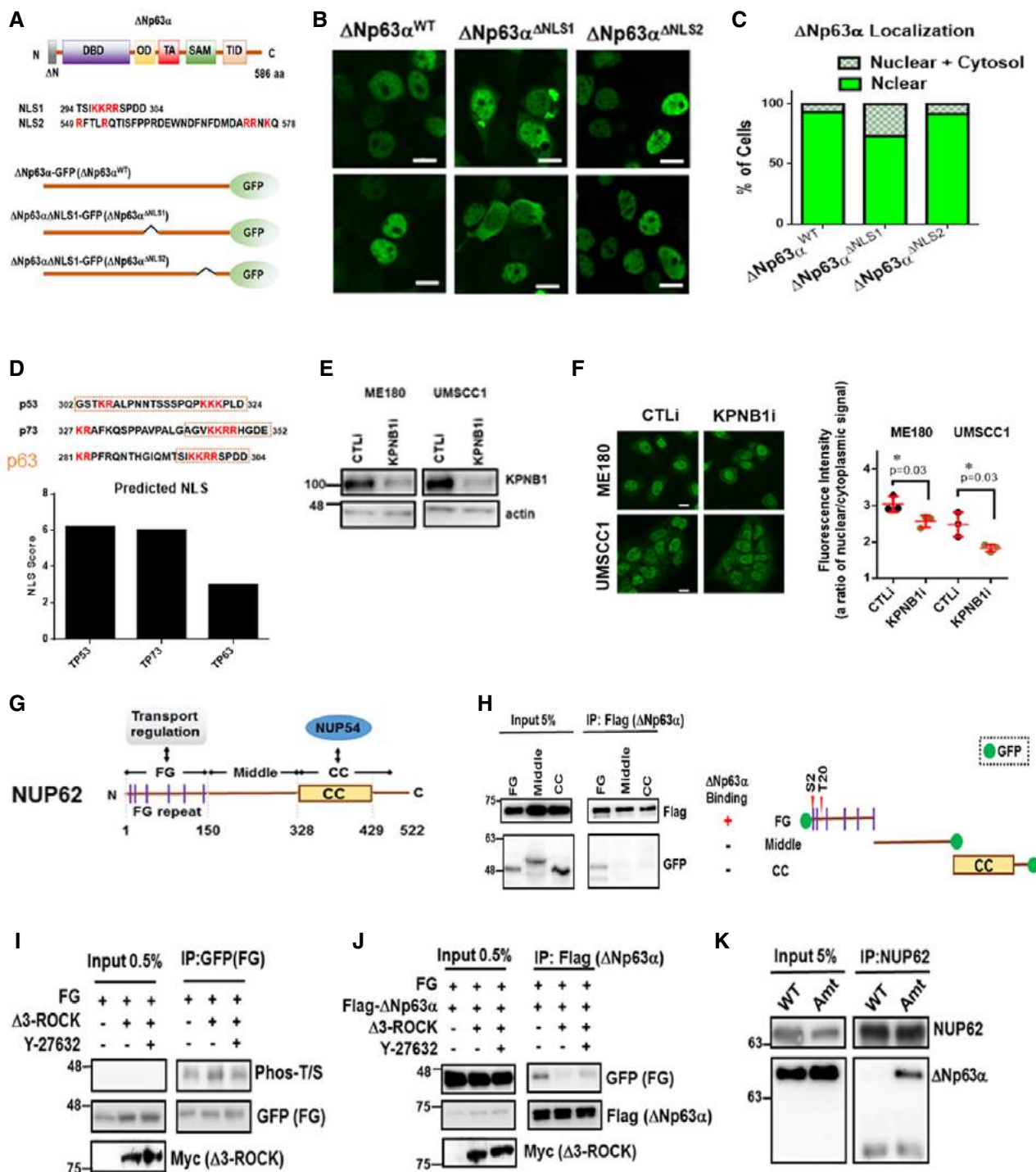


Figure 6.

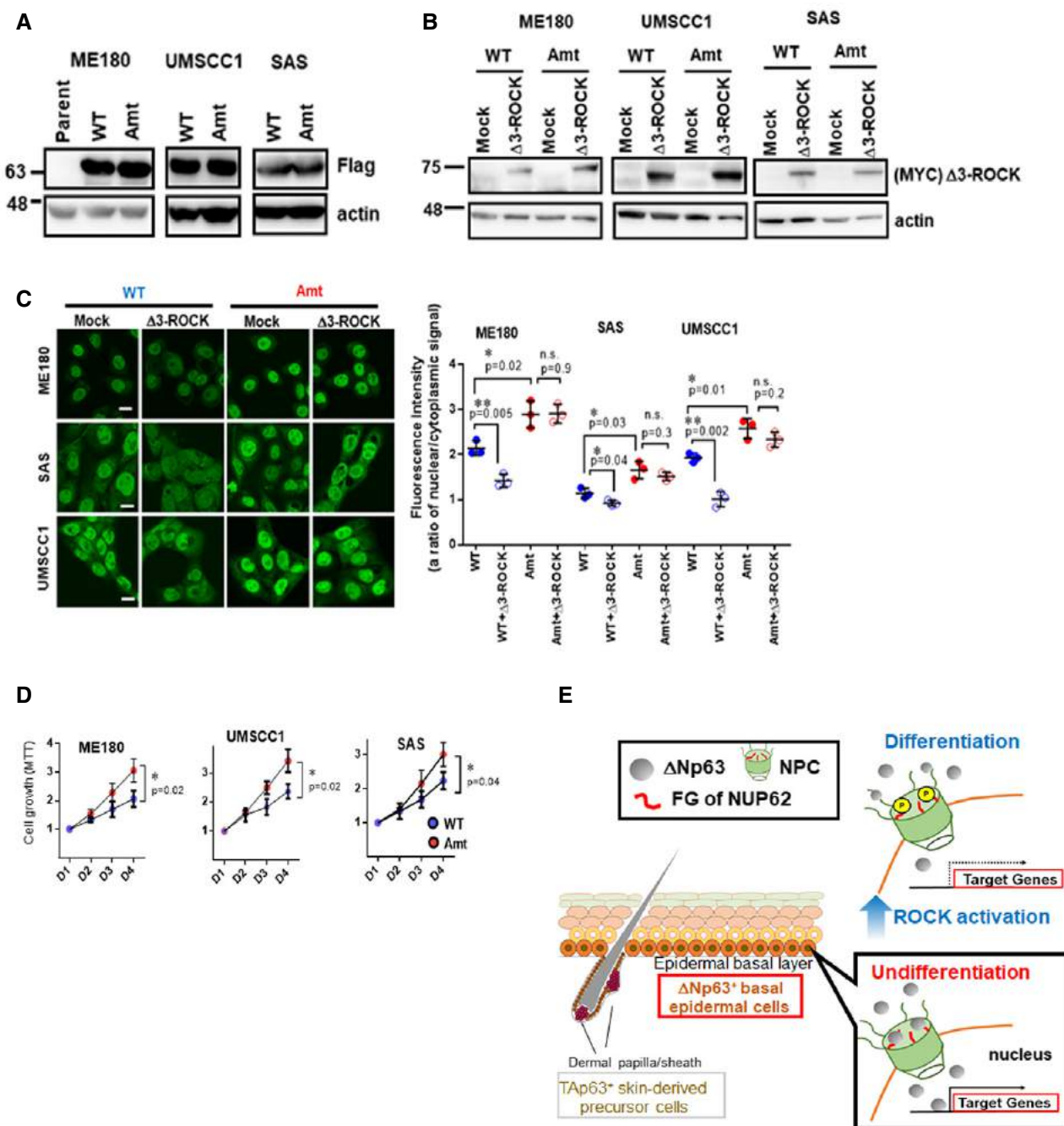


Figure 7. Δ Np63 α nuclear transport is mediated by the phosphorylation of FG domain of NUP62.

A, B Western blot analysis of ectopic WT and Amt NUP62 in SCC cells (A), and exogenous Δ 3-ROCK1 in those cells (B).

C Immunofluorescence confocal microscopic analysis of Δ Np63 α in SCC cells expressing either WT or Amt NUP62 after Δ 3-ROCK1 overexpression (72 h post transfection). Representative pictures (bar: 10 μ m) and quantification as a ratio of nuclear/cytoplasmic signals presented as a scatter plot with mean \pm SD from three independent experiments ($n = 3$). P values are based on unpaired two-tailed t -test with *indicating $P < 0.05$ and ** $P < 0.01$. n.s. indicate not significant.

D SCC cell lines expressing either WT or Amt NUP62 were subjected either to MTT assay. Data show mean \pm SD from three independent experiments ($n = 3$). P -values are based on unpaired two-tailed t -test with *indicating $P < 0.05$.

E Cross-section image of dermis and epidermis is modified from previous report [11]. Hypothetical model of NUP62 action in regulating cell fate.

Source data are available online for this figure.

Concordantly, we observed increased proliferative ability of SCC cells expressing Amt NUP62 compared to WT NUP62 based on both short-term proliferation assays and foci formation assays (Figs 7D,

and EV5C and D). Taken together, our data suggest a model in which NUP62 mediates Δ Np63 α nuclear transport to maintain proliferation and prevent differentiation of SCCs. ROCK pathway

negatively regulates this process by limiting Δ Np63 α -NUP62 interaction through the phosphorylation of the FG domain of NUP62 (Fig 7E).

Discussion

In this study, we showed novel trafficking regulation by NUP62 in human SCCs. Importantly, NUP62 regulated Δ Np63 α nuclear transport to prevent epidermal differentiation in SCCs. ROCK pathway inhibited the Δ Np63 α nuclear transport by reducing interaction between Δ Np63 α and NUP62 through the phosphorylation of the FG domain of NUP62.

Heterogeneity of NPC and the cell type-specific properties of some pore components have been reviewed [42]. Based on *in silico* analysis of NUPs transcripts across normal tissues, NUP62 expression levels were prominent in stratified epithelia tissues. We further determined that basal progenitor cells tend to express NUP62 in human skin tissue. In addition, SCC showed excessive levels of NUP62 compared to healthy tissues. We validated the function of NUP62 to maintain proliferative activity and suppress differentiation of SCCs, highlighting the cell type-specific role of NUP62 to regulate the cellular state of epidermal progenitor cells. Interestingly, Toda *et al* [63] recently uncovered the cell type-specific role of NUP153 in the control and maintenance of neural progenitor cells through bimodal transcriptional regulation. Present study demonstrated the role of NUP62 in SCC, however, how those NUPs cooperate in the regulation and maintenance of cell identity in different tissues and other types of cancer cells will be of interest.

We found that NUP62 regulated Δ Np63 α nuclear transport to maintain cellular undifferentiated status of SCCs. Importantly, p63 can be overexpressed including by genomic amplification, and the expression level of Δ Np63 α is a crucial clinical-pathological parameter affecting malignant potential of primary SCCs [1–4]. Furthermore, previous studies demonstrated the mechanistic action of Δ Np63 α in SCC [10,11]. For example, Δ Np63 α inhibits the activity of TAp73 [64] via transcriptional inhibition and, to a lesser extent, direct interaction between both proteins [65]. Therefore, attenuation of Δ Np63 α nuclear transport can serve as a new strategy to compromise its functions.

Nuclear transport receptors including KPNB1 are suggested to aid the shuttle of macromolecules larger than ~40 kDa. These NTRs bind to FG-NUPs, allowing the transport factors to cross NPC [66]. Here, we identified a candidate functional NLS (containing KKRR) on Δ Np63 α , which shows similarity with validated NLS on both p53 and p73 [58–60]. Previous studies demonstrated that destruction of KKRR on p53 and p73 almost completely blocked their nuclear accumulation [58–60]. In contrast, the effect of mutation of KKRR of Δ Np63 α was moderate in nuclear blockage. Δ Np63 α forms heterotetramers among p53 family members [10,11] and makes subcomplexes with cofactors such as p300 [67], which determine specificity and selectivity of downstream targets of Δ Np63. Therefore, NLS on interacting proteins may represent Δ Np63 α nuclear traffic to some extent. Identification of the p53 family protein complexes will enhance our understanding of the Δ Np63 α nuclear traffic system as well as selectivity of downstream targets of Δ Np63 α .

In addition, this study showed that the interaction between Δ Np63 α and FG domain of NUP62 is required for Δ Np63 α to enter

the nuclear space in SCCs. Importantly, ROCK1-dependent phosphorylation on FG domain resulted in attenuated interaction with Δ Np63 α as well as the nuclear transport ability. The ROCK1-specific inhibitor Y27632 was demonstrated to transform epithelial cells into continuously proliferating cells by increasing progenitor cell factors such as Δ Np63 α [20], suggesting that the ROCK pathway inhibits the self-renewal ability by suppressing Δ Np63 α expression. Previously, Kosako *et al* reported that ERK phosphorylation of the repeat region of FG of Nup50 reduced its affinity for particular NTRs, resulting in impaired nuclear migration of the NTRs [47]. Taken together, these findings suggest that transport ability and selectivity of NPC are controlled by kinase-dependent phosphorylation on the FG domain of FG-NUPs.

In summary, we show that high expression of NUP62 contributes to preventing epidermal differentiation of SCCs originating from stratified epithelia. Mechanistic studies reveal that NUP62 maintains Δ Np63 α entering NPC, whereas ROCK negatively regulates this process. Our results highlight cell type-specific role of NUP62 controlling systematically Δ Np63 α nuclear transport in SCCs. Our finding of convertible trafficking activity of NUP62 highlights the potential for therapeutic targeting of nuclear transport of this oncogene.

Materials and Methods

Cell culture

HEK293T, cervical SCC cell lines (HT3 and ME180), and head and neck SCC cell lines (UMSCC1, 93UV147, Ca9-22, and SAS) were maintained in Dulbecco's Modified Eagle Medium (DMEM) supplemented with 10% (vol/vol) fetal bovine serum (FBS) and 1% (vol/vol) penicillin/streptomycin (P/S) at 37°C, 5% CO₂ in a humidified atmosphere. Cell lines were authenticated by short tandem repeat analysis with the Geneprint 10 System Kit (Promega, B9510) in 2014.

Cell proliferation assay

Cells were seeded into a 96-well plate at 3,000 cells/well and cultured for the indicated time courses. Cell viability was assessed using the MTT (3-(4, 5-dimethylthiazol-2-yl)-2, 5-diphenyltetrazolium bromide) method. In brief, 10 μ l of 12 mM MTT solution was added into each well followed by 3-h incubation, which was stopped by adding 100 μ l of STOP solution (2% acetic acid, 16% SDS, 42% DMF). Samples were mixed thoroughly and measured at 570 nm for absorbance.

Foci formation assay

Squamous cell carcinoma cells were seeded into 6-well plates at 1,000 cells/well and cultured for 10 days, followed by fixation, staining with crystal violet and photographing the cells using LAS4000 (Fujifilm, Aichi, Japan). For quantification, the number of colonies (> 0.1 mm²) was determined using Multi Gauge Ver3.0 (Fujifilm).

Western blotting

Cells were lysed with lysis buffer [20 mM HEPES (pH 7.4), 350 mM sodium chloride, 1.5 mM magnesium chloride, 1 mM EGTA, 10%

(v/v) glycerol, 1% Triton X-100, a mixture of protease inhibitors (Roche), 0.2 mM sodium orthovanadate, and 1 mM phenylmethylsulfonyl fluoride]. Cell lysates or immunoprecipitation elutes were subjected to SDS-PAGE followed by conventional wet transfer. Membranes were incubated with antibodies and exposed to secondary horseradish peroxidase-conjugated antibodies (Millipore). Images were detected by using an LAS-4000 image analyzer (Fujifilm). Antibodies used in this study were listed in Table 1.

Immunoprecipitation

HEK293T cells were transiently transfected with the indicated mammalian expression plasmids and harvested 72 h after transfection. In the case of Y27632 treatment, transfected cells were incubated for 24 h before harvest. Indicated antibody was added and incubated overnight with each cell lysate at 4°C. Dynabeads Protein A/G (VERITUS, Tokyo, Japan) were added after washing for three

times with lysis buffer. After 2-h incubation, beads were washed four times in IP buffer (50 mM Tris, pH 7.6, 100 mM NaCl, 2 mM EDTA, 0.2% Nonidet P-40).

Tissue slide and immunofluorescent analysis

Human skin tissue sections (Kin08N004A5) were obtained from US Biomax Inc. The slides were deparaffinized and blocked with goat serum for 30 min at room temperature, followed by incubation with mouse anti-NUP62 (1:50; sc-48373, Santa Cruz) and rabbit anti-IVL (1:100; SAB4501594, Sigma) overnight at 4°C. After three washes, slides were incubated with Alexa 488- and Alexa 568-linked secondary antibody (Life Technologies) for 60 min. After three washes, Pro-Long Gold Antifade reagent (Life Technologies) was mounted onto samples and was examined by confocal microscopy (FluoView® FV10i, Olympus, objective $\times 60/1.2$).

Microscopic analysis using SCC cells

Cells on coverslips were incubated under indicated conditions. Cells were fixed for 10 min in 4% paraformaldehyde in PBS, then permeabilized with 0.3% Triton X-100 in PBS for 3 min at room temperature. Coverslips were incubated with indicated primary antibody for 2 h. Coverslips were washed three times and incubated with Alexa Fluor-conjugated secondary antibody (Life Technologies) for 1 h. After three washes, samples were mounted onto coverslips using Pro-Long Gold Antifade reagent (Life Technologies) and were examined by confocal microscopy (FluoView® FV10i, Olympus, objective $\times 60/1.2$). Nuclear $\Delta Np63\alpha$ signals were quantified with FV10i (Olympus).

cDNA vectors and siRNAs

The NUP62 fragment vectors have been described previously [68]. Constructs for overexpressing NUP62 were made by cloning cDNA derived from HaCaT into pLEX (Open Biosystems) using NotI/AgeI with C-terminal FLAG tag with the following primers: NUP62-F: 5'-ACAGTGGCGCCGCCACCACATGAGCGGGTTTAAT-3'; NUP62-R: 5'-GGCGACCGGTTTACTTGTCTCATCGTCTTTGTAGTCGTCGTCAGGTCGATCCG-3'. NUP62 CDS harboring mutations (S2A, T20A) was generated with the following primers: S2A-F1: 5'-ACAGTGGCGCCGCCACCACATGAGCGGGTTTAAT-3'; T20A-R: 5'-CTTTGCAGCGCCAAAC-3'; T20A-F: 5'-GTTTGGCGCTGCAAAG-3'; Mt3end-R: 5'-GGCGACCGGTTTACT. Two fragments were generated by PCR with S2A-F/T20A-R and T20A-F/Mt3end-R. After purification, these fragments were mixed and subjected to PCR using S2A-F/Mt3end-R. Constructs for overexpressing MYC-tag-fused $\Delta 3$ -ROCK1 were made by cloning cDNA derived from HaCaT into pLEX (Open Biosystems) using XhoI/AgeI sites. CDS-Seq was reported previously (National Center for Biotechnology Information (NCBI), see URL). The siRNAs targeting human nucleoporins are listed in Table 2, and scramble siRNA (D-001210-01) was purchased from Thermo Scientific.

Transfections, viral particle production, and infection

DNA and siRNA transfections were performed using Lipofectamine 2000 and Lipofectamine RNAiMAX (Life Technologies), respectively. Lentiviral particles were produced with the MISSION

Table 1. Antibodies.

Antibody	Company	Catalog #
β -actin	Santa Cruz Biotechnology	sc-47778
NUP107	Sigma-Aldrich	SAB3500333
NUP62	Sigma-Aldrich	N1163
NUP188	Abcam	ab86601
NUP54	Sigma-Aldrich	SAB1300588
TPR	Santa Cruz Biotechnology	sc-101294
p63(ΔN)	Biologend	619001
RanBP2	Santa Cruz Biotechnology	sc-74518
KPNB1	Abcam	ab2811
GFP	Wako	012-20461
GFP	Thermo Fisher Scientific	A6455
Flag	Sigma-Aldrich	F1804
Flag	MBL	PM020
Lamin A/C	Cell Signaling Technology	#2032
Fluorescent secondary antibody		
Goat anti-Rabbit IgG (H+L), Alexa Fluor 488	Thermo Fisher Scientific	A11034
Goat anti-Mouse IgG (H+L), Alexa Fluor 488	Thermo Fisher Scientific	A11029
Goat anti-Rabbit IgG (H+L), Rhodamine Red-X	Thermo Fisher Scientific	R6394
HRP-linked antibody		
anti-Mouse IgG	Cell Signaling Technology	7076S
anti-Rabbit IgG	Cell Signaling Technology	7074S
Protein A	GE Healthcare	N9120

Lentiviral Packaging System (Sigma-Aldrich). SCCs cells were transduced with the lentiviral particles in the presence of 8 µg/ml polybrene (Sigma-Aldrich) for 48 h.

cDNA preparation and quantitative Real-time RT-PCR assay

We used 500 ng RNA for cDNA preparation using ReverTra Ace[®] qPCR RT Master Mix (TOYOBO). Quantitative real-time RT-PCR was performed by SYBR[®] Premix Ex Taq[™] II (Takara) in a Thermal Cycler Dice[®] Real Time System (Takara) according to the manufacturer's instructions. The relative mRNA expression level of target genes was calculated using GAPDH as a loading control. The primers are listed in Table 3.

Microscopic analysis

Cells on coverslips were overexpressed Δ3-ROCK1 and then further incubated with either Y27632 or the CRM1 inhibitor for 24 h. For ΔNp63 staining, cells were fixed for 10 min in 4% paraformaldehyde in PBS, then permeabilized with 0.2% Triton X-100 in PBS for 20 min at room temperature. Permeabilization was proceeded before fixation in RanBP2/Flag dual staining [68]. Coverslips were incubated with indicated primary antibody for 2 h. Coverslips were washed three times and incubated with Alexa Fluor-conjugated secondary antibody (Life Technologies) for 1 h. After three washes, samples were mounted onto coverslips using Pro-Long Gold Antifade reagent (Life Technologies) and examined using confocal microscope (FluoView[®] FV10i, Olympus, objective ×60/1.2). Nuclear p63 signals were quantified with FV10i (Olympus).

DNA microarray analysis

Cyanine-3 (Cy3)-labeled cRNA was prepared from 0.2 µg RNA using the Low Input Quick Amp Labeling Kit (Agilent Technologies) according to the manufacturer's instructions, followed by RNeasy column purification (QIAGEN, Valencia, CA). Samples were hybridized to Whole Human Genome microarray 4 × 44 K Ver. 2.0 (G4845A, Agilent Technologies). The slides were scanned on the Agilent DNA Microarray Scanner (G2539A) using one color scan setting for 4 × 44 k array slides. The scanned images were analyzed with Feature Extraction Software 11.0.1.1 (Agilent) using default parameters (protocol AgilentHD_GX_1Color and Grid: 026652_D_F_20120130) to obtain background subtracted and

spatially detrended Processed Signal intensities. The raw data have been deposited in the Gene Expression Omnibus (GEO) database, under number GSE103991.

Table 3. Primers.

	Sequence (5'–3')
GAPDH-F	GTCAGTGGTGACCTGACCT
GAPDH-R	AGGGGTCTACATGGCAACTG
EGFR-F	TAACAAGCTCACGCGAGTTGG
EGFR-R	GTTGAGGGCAATGAGGACAT
ADA-F	GACCCGCTCATCTTCAAGTC
ADA-R	GGTCGAGAAGCTCCCTCTTT
PERP-F	CATGCTCTTCTGTGGCTTCA
PERP-R	AAAGCCGTAGGCCAGTTAT
EDAR-F	GTATGCCAACGTGTGGAG
EDAR-R	CCCAATCTCATCCCTCTTCA
ZNF750-F	TAAGCCTCAATGTTGTGAAC
ZNF750-R	CTGATTTCTTGAGAGGTTG
WWC1-F	CGCTGACGGAGAGTTAAAG
WWC1-R	GCTGAAGTGGAGGAGTCCAG
PUMA-F	GACGACCTCAACGCACAGTA
PUMA-R	CACCTAATGGGCTCCATCT
CDKN1A-F	GACACCACTGGAGGGTACT
CDKN1A-R	CTGCCTCTCCCAACTCAT
SPRR1B-F	TATTCCTCTTTCACACCAG
SPRR1B-R	TCCTTGGTTTTGGGGATG
IVL-F	TTACTGTGAGTCTGTTGAC
IVL-R	TGTTTCATTTGCTCCTGATG
NUP62-F	ACATCGATGCACAGCTCAAAG
NUP62-R	ACTGCAGTGAGTCCATGTGC
TP63-F	ACCTGGAAAACATGCCAGA
TP63-R	ACGAGGAGCCGTTCTGAATC
LOR-F	GAGTAGCCGCAGCCAGAAC
LOR-R	CTCCTCACTCACCTTCTCTG
FLG-F	AATTTGCGCAAATCCTGAAG
FLG-R	CTTGAGCCAACCTGAATACC
Gli2-F	CAGCTGCGCAAACACATGA
Gli2-R	TTGAGTGACTTGAGCTTCTCTTCT
IHH-F	CGGCTTTGACTGGGTGTATT
IHH-R	GAAAATGAGCACATCGCTGA
Smad7-F	GTGGATGGTGTGTGGGTGTA
Smad7-R	CAAAGCTGATCTGCACGGTA
FASN-F	CTGGCTCAGCACCTCTATCC
FASN-R	CAGGTTGTCCCTGTGATCCT
SKT11-F	GCTCTTACGGCAAAGTGAAG
SKT11-R	TTTTGTCCGTAACCTCCTC
FN1-F	ACCAACCTACGGATGACTCG
FN1-R	GCTCATCATCTGGCCATTTT

Table 2. siRNAs oligonucleotides.

siRNA	Company	Catalog #
Control	Sigma-Aldrich	SIC001
NUP107	Santa Cruz Biotechnology	sc-45343
NUP85	Life Technologies	4392420
NUP62	Sigma-Aldrich	SASI_Hs01_00038069
NUP54	Santa Cruz Biotechnology	sc-92940
NUP188	Santa Cruz Biotechnology	sc-92946
KPNB1	Sigma-Aldrich	SASI_Hs01_00101673
TPR	Santa Cruz Biotechnology	sc-45343

Bioinformatics and data analysis

NUP62 mRNA expression across normal tissues was examined from The Human Protein Atlas (see URLs). The expression of NUP62, NUP107, NUP85, NUP54, NUP188, TPR, SPRR1B, and IVL mRNA in HNSCC was from The Cancer Genome Atlas (TCGA) through Cancer RNA-Seq Nexus or cBioportal (see URLs). NUP62 protein expression levels in stratified epithelia tissues were from Human Protein Atlas (see URLs). Gene Ontology (GO) analysis and pathway were performed via ConsensusPathDB (see URLs). Gene Set Enrichment Analysis (GSEA) was performed with GSEA v2.2.2 software (see URLs). Phosphorylated sites in NUP62 were from PhosphoSitePlus (see URLs).

Statistical analyses

Following assays: cell proliferation assay, anchorage-dependent colony formation assay, and real-time RT-PCR analysis were performed in triplicates ($n = 3$) and independently replicated 2–4 times. Data are the average of independent experiments ($n = 2$ or 3). Unpaired two-tailed *t*-test was performed by GraphPad Prism in the statistical analysis of the following assays: cell proliferation assay, anchorage-dependent colony formation assay, and real-time RT-PCR analysis. $P < 0.05$ was considered statistically significant. When control group is considered as 100%, one sample *t*-test was performed using GraphPad QuickCalcs (see URLs).

URLs

The Cancer Genome Atlas (TCGA), <http://cancergenome.nih.gov/>; cBio Cancer Genomics Portal, <http://www.cbioportal.org/>; Human Protein Atlas, <http://www.proteinatlas.org/>; Gene Expression Omnibus (GEO), <http://syslab4.nchu.edu.tw/>; Cancer RNA-Seq Nexus, <http://portals.broadinstitute.org/ccle/>; Gene Set Enrichment Analysis (GSEA), <http://software.broadinstitute.org/gsea/>; ConsensusPathDB, <http://consensuspathdb.org/>; PhosphoSitePlus, <http://www.phosphosite.org/homeAction.action>. GraphPad QuickCalcs, <http://graphpad.com/quickcalcs/OneSampleT1.cfm>; NCBI, <https://www.ncbi.nlm.nih.gov/>.

Expanded View for this article is available online.

Acknowledgements

We thank Takayuki Dowaki, Kie Sakai, and Ryota Tsukahara for technical support. This work was funded by an Infiniti Grant and in part by Grants-in-Aid for scientific research (JSPS KAKENHI Grant Number 17K16332) and (JSPS KAKENHI Grant Number 80292423) from the Japan Society for Promotion of Science. This research was supported by the grant provided by The Ichiro Kanehara Foundation. This work was also supported by World Premier International Research Center Initiative (WPI), MEXT, Japan.

Author contributions

MH and RWW initiated the research; MH, D-CL, and RWW developed methodology; MH, AK, Y-Y, LX, FRPD, MSM, and H performed experiments and collected data; S-iH performed micro-array analysis; MM-H performed tissue-immunofluorescence analysis; MH, D-CL, MN, HPK, and RWW analyzed and interpreted data; MH, D-CL, HPK, and RWW wrote, reviewed, and revised the manuscripts with input from all authors; MH and RWW supervised the study.

Conflict of interest

The authors declare that they have no conflict of interest.

References

1. Cancer Genome Atlas Network (2015) Comprehensive genomic characterization of head and neck squamous cell carcinomas. *Nature* 517: 576–582
2. Lin DC, Hao JJ, Nagata Y, Xu L, Shang L, Meng X, Sato Y, Okuno Y, Varela AM, Ding LW *et al* (2014) Genomic and molecular characterization of esophageal squamous cell carcinoma. *Nat Genet* 46: 467–473
3. Lee CS, Bhaduri A, Mah A, Johnson WL, Ungewickell A, Aros CJ, Nguyen CB, Rios EJ, Sibrashvili Z, Straight A *et al* (2014) Recurrent point mutations in the kinetochore gene KNSTRN in cutaneous squamous cell carcinoma. *Nat Genet* 46: 1060–1062
4. Cancer Genome Atlas Research Network, Analysis Working Group: Asan University, BC Cancer Agency, Brigham and Women's Hospital, Broad Institute, Brown University, Case Western Reserve University, Dana-Farber Cancer Institute, Duke University, Greater Poland Cancer Centre *et al* (2017) Integrated genomic characterization of oesophageal carcinoma. *Nature* 541: 169–175
5. Mills AA, Zheng B, Wang XJ, Vogel H, Roop DR, Bradley A (1999) p63 is a p53 homologue required for limb and epidermal morphogenesis. *Nature* 398: 708–713
6. Yang A, Schweitzer R, Sun D, Kaghad M, Walker N, Bronson RT, Tabin C, Sharpe A, Caput D, Crum C *et al* (1999) p63 is essential for regenerative proliferation in limb, craniofacial and epithelial development. *Nature* 398: 714–718
7. Keyes WM, Wu Y, Vogel H, Guo X, Lowe SW, Mills AA (2005) p63 deficiency activates a program of cellular senescence and leads to accelerated aging. *Genes Dev* 19: 1986–1999
8. Senoo M, Pint F, Crum CP, McKeon F (2007) p63 is essential for the proliferative potential of stem cells in stratified epithelia. *Cell* 129: 523–536
9. Yang A, McKeon F (2000) P63 and P73: P53 mimics, menaces and more. *Nat Rev Mol Cell Biol* 1: 199–207
10. Su X, Chakravarti D, Flores ER (2013) p63 steps into the limelight: crucial roles in the suppression of tumorigenesis and metastasis. *Nat Rev Cancer* 13: 136–143
11. Botchkarev VA, Flores ER (2014) p53/p63/p73 in the epidermis in health and disease. *Cold Spring Harb Perspect Med* 4: pii: a015248
12. Melino G, Memmi EM, Pelicci PG, Bernassola F (2015) Maintaining epithelial stemness with p63. *Sci Signal* 8: re9
13. Yang A, Kaghad M, Wang Y, Gillett E, Fleming MD, Dötsch V, Andrews NC, Caput D, McKeon F (1998) p63 is the molecular switch for initiation of an epithelial stratification program. *Mol Cell* 2: 305–316
14. Kouwenhoven EN, Oti M, Niehues H, van Heeringen SJ, Schalkwijk J, Stunnenberg HG, van Bokhoven H, Zhou H (2015) Transcription factor p63 bookmarks and regulates dynamic enhancers during epidermal differentiation. *EMBO Rep* 16: 863–878
15. Pellegrini G, Dellambra E, Golisano O, Martinelli E, Fantozzi I, Bondanza S, Ponzin D, McKeon F, De Luca M (2001) p63 identifies keratinocyte stem cells. *Proc Natl Acad Sci USA* 98: 3156–3161
16. Leonard MK, Kommagani R, Payal V, Mayo LD, Shamma HN, Kadakia MP (2011) $\Delta Np63\alpha$ regulates keratinocyte proliferation by controlling PTEN expression and localization. *Cell Death Differ* 18: 1924–1933

17. Rossi M, Aqeilan RI, Neale M, Candi E, Salomoni P, Knight RA, Croce CM, Melino G (2006) The E3 ubiquitin ligase Itch controls the protein stability of p63. *Proc Natl Acad Sci USA* 103: 12753–12758
18. Yugawa T, Nishino K, Ohno S, Nakahara T, Fujita M, Goshima N, Umezawa A, Kiyono T (2013) Noncanonical NOTCH signaling limits self-renewal of human epithelial and induced pluripotent stem cells through ROCK activation. *Mol Cell Biol* 33: 4434–4447
19. McMullan R, Lax S, Robertson VH, Radford DJ, Broad S, Watt FM, Rowles A, Croft DR, Olson MF, Hotchin NA (2003) Keratinocyte differentiation is regulated by the Rho and ROCK signaling pathway. *Curr Biol* 13: 2185–2189
20. Suprynovicz FA, Upadhyay G, Krawczyk E, Kramer SC, Hebert JD, Liu X, Yuan H, Cheluvvaraju C, Clapp PW, Boucher RC Jr et al (2012) Conditionally reprogrammed cells represent a stem-like state of adult epithelial cells. *Proc Natl Acad Sci USA* 109: 20035–20040
21. Yugawa T, Narisawa-Saito M, Yoshimatsu Y, Haga K, Ohno S, Egawa N, Fujita M, Kiyono T (2010) DeltaNp63alpha repression of the Notch1 gene supports the proliferative capacity of normal human keratinocytes and cervical cancer cells. *Cancer Res* 70: 4034–4044
22. Ramsey MR, He L, Forster N, Ory B, Ellisen LW (2011) Physical association of HDAC1 and HDAC2 with p63 mediates transcriptional repression and tumor maintenance in squamous cell carcinoma. *Cancer Res* 71: 4373–4379
23. Keyes WM, Pecoraro M, Aranda V, Vernersson-Lindahl E, Li W, Vogel H, Guo X, Garcia EL, Michurina TV, Enikolopov G et al (2011) Δ Np63 α is an oncogene that targets chromatin remodeler Lsh to drive skin stem cell proliferation and tumorigenesis. *Cell Stem Cell* 8: 164–176
24. Ramsey MR, Wilson C, Ory B, Rothenberg SM, Faquin W, Mills AA, Ellisen LW (2013) FGFR2 signaling underlies p63 oncogenic function in squamous cell carcinoma. *J Clin Invest* 123: 3525–3538
25. Saladi SV, Ross K, Karaayvaz M, Tata PR, Mou H, Rajagopal J, Ramaswamy S, Ellisen LW (2017) ACTL6A is co-amplified with p63 in squamous cell carcinoma to drive YAP activation, regenerative proliferation, and poor prognosis. *Cancer Cell* 31: 35–49
26. Carroll DK, Carroll JS, Leong CO, Cheng F, Brown M, Mills AA, Brugge JS, Ellisen LW et al (2006) p63 regulates an adhesion programme and cell survival in epithelial cells. *Nat Cell Biol* 8: 551–561
27. Tordella L, Koch S, Salter V, Pagotto A, Doondeea JB, Feller SM, Ratnayaka I, Zhong S, Goldin RD, Lozano G et al (2013) ASPP2 suppresses squamous cell carcinoma via RelA/p65-mediated repression of p63. *Proc Natl Acad Sci USA* 110: 17969–17974
28. Funasaka T, Wong RW (2011) The role of nuclear pore complex in tumor microenvironment and metastasis. *Cancer Metastasis Rev* 30: 239–251
29. Simon DN, Rout MP (2014) Cancer and the nuclear pore complex. *Adv Exp Med Biol* 773: 285–307
30. Wong RW (2015) Nuclear pore complex: from structural view to chemical tools. *Chem Biol* 22: 1285–1287
31. Ibarra A, Hetzer MW (2015) Nuclear pore proteins and the control of genome functions. *Genes Dev* 29: 337–349
32. Hoelz A, Glavy JS, Beck M (2016) Toward the atomic structure of the nuclear pore complex: when top down meets bottom up. *Nat Struct Mol Biol* 23: 624–630
33. Sakuma S, D'Angelo MA (2017) The roles of the nuclear pore complex in cellular dysfunction, aging and disease. *Semin Cell Dev Biol* 68: 72–84
34. Terry LJ, Wentz SR (2009) Flexible gates: dynamic topologies and functions for FG nucleoporins in nucleocytoplasmic transport. *Eukaryot Cell* 8: 1814–1827
35. Mohamed MS, Kobayashi A, Taoka A, Watanabe-Nakayama T, Kikuchi Y, Hazawa M, Minamoto T, Fukumori Y, Kodera N, Uchihashi T et al (2017) High-speed atomic force microscopy reveals loss of nuclear pore resilience as a dying code in colorectal cancer cells. *ACS Nano* 11: 5567–5578
36. Lupu F, Alves A, Anderson K, Doye V, Lacy E (2008) Nuclear pore composition regulates neural stem/progenitor cell differentiation in the mouse embryo. *Dev Cell* 14: 831–842
37. D'Angelo MA, Gomez-Cavazos JS, Mei A, Lackner DH, Hetzer MW (2012) A change in nuclear pore complex composition regulates cell differentiation. *Dev Cell* 22: 446–458
38. Gomez-Cavazos JS, Hetzer MW (2015) The nucleoporin gp210/Nup210 controls muscle differentiation by regulating nuclear envelope/ER homeostasis. *J Cell Biol* 208: 671–681
39. Jacinto FV, Benner C, Hetzer MW (2015) The nucleoporin Nup153 regulates embryonic stem cell pluripotency through gene silencing. *Genes Dev* 29: 1224–1238
40. Ibarra A, Benner C, Tyagi S, Cool J, Hetzer MW (2016) Nucleoporin-mediated regulation of cell identity genes. *Genes Dev* 30: 2253–2258
41. Raices M, Bukata L, Sakuma S, Borlido J, Hernandez LS, Hart DO, D'Angelo MA (2017) Nuclear pores regulate muscle development and maintenance by assembling a localized Mef2C complex. *Dev Cell* 41: 540–554
42. Raices M, D'Angelo MA (2012) Nuclear pore complex composition: a new regulator of tissue-specific and developmental functions. *Nat Rev Mol Cell Biol* 13: 687–699
43. Testoni B, Borrelli S, Tenedini E, Alotto D, Castagnoli C, Piccolo S, Tagliafico E, Ferrari S, Viganò MA, Mantovani R (2006) Identification of new p63 targets in human keratinocytes. *Cell Cycle* 5: 2805–2811
44. Sbsia E, Mastropasqua G, Lefkimmatis K, Caratozzolo MF, D'Erchia AM, Tullo A (2006) Connecting p63 to cellular proliferation: the example of the adenosine deaminase target gene. *Cell Cycle* 5: 205–212
45. Ihrle RA, Marques MR, Nguyen BT, Horner JS, Papazoglu C, Bronson RT, Mills AA, Attardi LD (2005) Perp is a p63-regulated gene essential for epithelial integrity. *Cell* 120: 843–856
46. Laurikkala J, Mikkola ML, James M, Tummers M, Mills AA, Thesleff I (2006) p63 regulates multiple signalling pathways required for ectodermal organogenesis and differentiation. *Development* 133: 1553–1563
47. Sen GL, Boxer LD, Webster DE, Bussat RT, Qu K, Zarnegar BJ, Johnston D, Siprashvili Z, Khavari PA (2012) ZNF750 is a p63 target gene that induces KLF4 to drive terminal epidermal differentiation. *Dev Cell* 22: 669–677
48. Hazawa M, Lin DC, Handral H, Xu L, Chen Y, Jiang YY, Mayakonda A, Ding LW, Meng X, Sharma A et al (2017) ZNF750 is a lineage-specific tumour suppressor in squamous cell carcinoma. *Oncogene* 36: 2243–2254
49. Westfall MD, Mays DJ, Sniezek JC, Pietenpol JA (2003) The Delta Np63 alpha phosphoprotein binds the p21 and 14-3-3 sigma promoters *in vivo* and has transcriptional repressor activity that is reduced by Hay-Wells syndrome-derived mutations. *Mol Cell Biol* 23: 2264–2276
50. Li N, Singh S, Cherukuri P, Li H, Yuan Z, Ellisen LW, Wang B, Robbins D, DiRenzo J (2008) Reciprocal intraepithelial interactions between TP63 and hedgehog signaling regulate quiescence and activation of progenitor elaboration by mammary stem cells. *Stem Cells* 26: 1253–1264
51. Memmi EM, Sanarico AG, Giacobbe A, Peschiaroli A, Frezza V, Cicalese A, Pisati F, Tosoni D, Zhou H, Tonon G et al (2015) p63 sustains self-renewal of mammary cancer stem cells through regulation of Sonic Hedgehog signaling. *Proc Natl Acad Sci USA* 112: 3499–3504

52. De Rosa L, Antonini D, Ferone G, Russo MT, Yu PB, Han R, Missero C (2009) p63 Suppresses non-epidermal lineage markers in a bone morphogenetic protein-dependent manner via repression of Smad7. *J Biol Chem* 284: 30574–30582
53. Su X, Gi YJ, Chakravarti D, Chan IL, Zhang A, Xia X, Tsai KY, Flores ER (2012) TAp63 is a master transcriptional regulator of lipid and glucose metabolism. *Cell Metab* 16: 511–525
54. Kosako H, Yamaguchi N, Aranami C, Ushiyama M, Kose S, Imamoto N, Taniguchi H, Nishida E, Hattori S (2009) Phosphoproteomics reveals new ERK MAP kinase targets and links ERK to nucleoporin-mediated nuclear transport. *Nat Struct Mol Biol* 16: 1026–1035
55. Iwanicki MP, Vomastek T, Tilghman RW, Martin KH, Banerjee J, Wedegaertner PB, Parsons JT (2008) FAK, PDZ-RhoGEF and ROCKII cooperate to regulate adhesion movement and trailing-edge retraction in fibroblasts. *J Cell Sci* 121: 895–905
56. Ishizaki T, Naito M, Fujisawa K, Maekawa M, Watanabe N, Saito Y, Narumiya S (1997) p160ROCK, a Rho-associated coiled-coil forming protein kinase, works downstream of Rho and induces focal adhesions. *FEBS Lett* 404: 118–124
57. Christie M, Chang CW, Róna G, Smith KM, Stewart AG, Takeda AA, Fontes MR, Stewart M, Vértessy BG, Forwood JK et al (2016) Structural biology and regulation of protein import into the nucleus. *J Mol Biol* 428: 2060–2090
58. Liang SH, Clarke MF (1999) The nuclear import of p53 is determined by the presence of a basic domain and its relative position to the nuclear localization signal. *Oncogene* 18: 2163–2166
59. Liang SH, Clarke MF (1999) A bipartite nuclear localization signal is required for p53 nuclear import regulated by a carboxyl-terminal domain. *J Biol Chem* 274: 32699–32703
60. Inoue T, Stuart J, Leno R, Maki CG (2002) Nuclear import and export signals in control of the p53-related protein p73. *J Biol Chem* 277: 15053–15060
61. Solmaz SR, Chauhan R, Blobel G, Melčák I (2011) Molecular architecture of the transport channel of the nuclear pore complex. *Cell* 147: 590–602
62. Sahoo MR, Gaikwad S, Khuperkar D, Ashok M, Helen M, Yadav SK, Singh A, Magre I, Deshmukh P, Dhanvijay S et al (2017) Nup358 binds to AGO proteins through its SUMO-interacting motifs and promotes the association of target mRNA with miRISC. *EMBO Rep* 18: 241–263
63. Toda T, Hsu JY, Linker SB, Hu L, Schafer ST, Mertens J, Jacinto FV, Hetzer MW, Gage FH (2017) Nup153 interacts with Sox2 to enable bimodal gene regulation and maintenance of neural progenitor cells. *Cell Stem Cell* 21: 618–634.e7
64. Rocco JW, Leong CO, Kuperwasser N, DeYoung MP, Ellisen LW (2006) p63 mediates survival in squamous cell carcinoma by suppression of p73-dependent apoptosis. *Cancer Cell* 9: 45–56
65. Gebel J, Luh LM, Coutandin D, Osterburg C, Löhr F, Schäfer B, Frombach AS, Sumyk M, Buchner L, Krojer T et al (2016) Mechanism of TAp73 inhibition by Δ Np63 and structural basis of p63/p73 hetero-tetramerization. *Cell Death Differ* 23: 1930–1940
66. Schoch RL, Kapinos LE, Lim RY (2012) Nuclear transport receptor binding avidity triggers a self-healing collapse transition in FG-nucleoporin molecular brushes. *Proc Natl Acad Sci USA* 109: 16911–16916
67. MacPartlin M, Zeng S, Lee H, Stauffer D, Jin Y, Thayer M, Lu H (2005) p300 regulates p63 transcriptional activity. *J Biol Chem* 280: 30604–30610
68. Hashizume C, Moyori A, Kobayashi A, Yamakoshi N, Endo A, Wong RW (2013) Nucleoporin Nup62 maintains centrosome homeostasis. *Cell Cycle* 12: 3804–3816